On the propagation of particulate gravity currents in circular and semi-circular channels partially filled with homogeneous or stratified ambient fluid

T. Zemach,[1] L. Chiapponi,[2] D. Petrolo,[2] M. Ungarish,[3] S. Longo,[2,a)] and V. Di Federico[4]
[1]*Department of Computer Science, Tel-Hai College, Tel-Hai, Israel*
[2]*Dipartimento di Ingegneria Civile e Architettura (DIA), Università di Parma, Parco Area delle Scienze, 181/A, 43124 Parma, Italy*
[3]*Department of Computer Science, Technion, Israel Institute of Technology, Haifa 32000, Israel*
[4]*Dipartimento di Ingegneria Civile, Chimica, Ambientale e dei Materiali (DICAM), Università di Bologna, Viale Risorgimento, 2, 40136 Bologna, Italy*

(Received 11 July 2017; accepted 4 October 2017; published online 27 October 2017)

We present a combined theoretical-experimental investigation of particle-driven gravity currents advancing in circular cross section channels in the high-Reynolds number Boussinesq regime; the ambient fluid is either homogeneous or linearly stratified. The predictions of the theoretical model are compared with experiments performed in lock–release configuration; experiments were performed with conditions of both full-depth and partial-depth locks. Two different particles were used for the turbidity current, and the full range $0 \leq S \leq 1$ of the stratification parameter was explored ($S = 0$ corresponds to the homogeneous case and $S = 1$ when the density of the ambient fluid and of the current are equal at the bottom). In addition, a few saline gravity currents were tested for comparison. The results show good agreement for the full-depth configuration, with the initial depth of the current in the lock being equal to the depth of the ambient fluid. The agreement is less good for the partial-depth cases and is improved by the introduction of a simple adjustment coefficient for the Froude number at the front of the current and accounting for dissipation. The general parameter dependencies and behaviour of the current, although influenced by many factors (e.g., mixing and internal waves), are well predicted by the relatively simple model. *Published by AIP Publishing.*
https://doi.org/10.1063/1.4995388

I. INTRODUCTION

Gravity currents (GCs) carrying suspended particulate matter are commonly termed turbidity currents (hereafter TCs) and are a model for several flows occurring in natural settings both above and under water. TCs are generated during volcanic eruptions, when clouds of erupted material evolve in turbidity flows and advance down the mountain side in the form of pyroclastic avalanches. Frequently, self-triggered TCs develop underwater and propagate along submarine canyons. Other common types of TCs in the atmosphere are the dry-snow avalanches, further classified as flow avalanches and air-borne powder snow avalanches by Simpson.[33] Turbidity currents in lakes and oceans are considered as a major agent in shaping the morphology of submarine canyons[15] and in damaging telegraph cables after earthquakes.[11,33] Ancient deposits of TCs have often become oil reservoirs.[30] TCs are also a threat if the sediments and/or the interstitial fluid are polluted; Normark and Dickson[29] and Hay[10] documented turbidity currents in lakes generated by the discharge of mine tailings, which are considered the source of several diseases.[6] A general overview of particulate GCs is presented by Huppert[14] and Kneller and Buckee.[16]

In standard GCs, density inhomogeneities are caused by dissolved salts ("saline GCs") or by temperature differences, whilst in TCs they are due to suspended particles. The different source of density differences does not prevent applying to TCs most of the analyses developed for saline GCs.[32] However, the coupling with sediment dynamics renders the analysis more complex: a net mass exchange with the bed is expected in the presence of particulate matter, in turn producing a spatial and temporal variation of the buoyancy of the current. In most cases, sediment fallout entails a reduction of buoyancy; the reverse is true, and the buoyancy increases (sometimes in an explosive manner, see the work of Seymour[31]) when particle entrainment is exceeding deposits. At any rate, the settling speed of the particles becomes a parameter in the model and governs the overall evolution of TCs.

Several theoretical studies and experimental campaigns are available on the behaviour of TCs flowing into a homogeneous ambient fluid. Bonnecaze *et al.*[4] first presented a single-layer model for plane TCs flowing into a deep ambient fluid and refined their model with a two-layer approach to take into account the flow in the ambient fluid for shallow surroundings; modeling predictions were confirmed by experiments in a horizontal tank of rectangular cross section. Constant flux tests were performed for plane currents by Garcia[8] to validate a layer-averaged model and by Altinakar *et al.*[1] to evaluate

a)Author to whom correspondence should be addressed: sandro.longo@unipr.it

velocity and concentration distributions using different sediment mixtures. Asymptotic and box-model solutions for two-dimensional TC propagation were derived by Hogg *et al.*[13] The peculiar effects of an interstitial buoyant fluid on sediment-laden gravity currents of planar geometry were conceptually identified and demonstrated experimentally by Sparks *et al.*[34] The modeling and experimental efforts of Bonnecaze *et al.*[3] focused on propagation in axisymmetric geometry, adopting either a constant volume or constant flux boundary condition.

In all experiments cited, the walls of the tank were rigid and only deposition of sediments was allowed. Mohrig and Buttles[25] made experiments to check the attitude of TCs to spread in channelized, quasi-channelized, and unconfined flows in the presence of pre-existing channels, finding that the ratio between the thickness of the current and the pre-existing channel depth is the main parameter controlling the current's evolution.

It is a matter of evidence that the shape of the cross section of the channel plays a significant role in the spreading of GCs in general and of TCs in particular. Natural channels are seldom regular and often show a clear non-rectangular cross section; if the walls of the channel are convergent, the final position of sediments is also dictated by the geometry since particles tend to fill the lowest part of the channel. This phenomenon is particularly relevant for a triangular, but is also evident for a circular cross section, which is the shape of the channel in the present experiments. Monaghan *et al.*[27] performed lock-exchange experiments in a V-shaped channel, comparing their results with the predictions of a box model. Refined two-layer models of saline GCs accounting for the channel shape were developed by Ungarish,[39] obtaining satisfactory agreement with the experiments by Monaghan *et al.*[27] and by Marino and Thomas.[20] Further theoretical and experimental analyses have been developed by Ungarish *et al.*[42] and Longo *et al.*[18,19] For TCs, Monaghan *et al.*[26] performed lock-exchange experiments in a V-shaped channel; Zemach[44] developed a one-layer theory valid for propagation within a generic non-rectangular cross section and performed numerical simulations to illustrate the results obtained; Mériaux *et al.*[24] performed experiments in V-shaped channels and compared them successfully with the general theory; Mériaux and Kurz-Besson[23] theoretically and experimentally studied currents carrying polydisperse particles along a V-shaped valley and found a criterion of equivalence with monogranular TCs: the mass-weighted mean size of the initial distribution of particles is representative of the suspension (also in terms of runout length) provided a sufficient number of size classes are considered.

In this paper, a novel series of experiments is devoted to particulate gravity currents advancing in a horizontal channel of circular cross section, under lock–release (constant volume) conditions, with full-depth and partial-depth configurations. The experiments are original and extend past results in similar conditions.

A second factor affecting the spreading characteristics of GCs is the ambient fluid, which can be either homogeneous or density stratified. In the latter condition, a new unexpected phenomenon takes place, like the formation of internal waves.[43] Theoretical models which take to account the ambient fluid stratification were developed by Ungarish and Huppert[41] and Ungarish,[35] with an extension to a two-layer approach by Flynn *et al.*[7] and a further extension to a stratified current advancing in a stratified ambient fluid by Ungarish.[38] The experimental validation of these models is reported in the work of Maxworthy *et al.*[22] for a rectangular cross section and in the work of Longo *et al.*[17] for a circular cross section. The experiments show the role of the internal waves, which affect the GC evolution with a clear separation of regimes between sub-critical and super-critical conditions (referred to as the front speed and the phase celerity of the internal waves).

The coexistence of particulates and density stratified ambient fluid is a new topic that deserves attention. In estuarine areas, fresh water loaded with suspended sediments encounters salty seawater, often exhibiting stratification, and progressively reduces its density due to settling of the particles, eventually facilitated by flocculation. The theoretical model for a TC advancing in a linearly stratified ambient fluid, and its experimental validation, constitutes the second original contribution of the present paper. Also this second set of experiments is performed in a horizontal channel of circular cross section under lock–release conditions.

The theoretical model is deliberately as simple as possible in order to reduce the number of parameters and to validate the capability of prediction even if some important physical aspects are neglected. Clearly, the adoption of a simple model may affect its ability to make insightful prediction. A more stringent comparison with the experiments requires the inclusion of mixing and entrainment, of resistance, and of the stratification and dispersion of sediments, together with the modeling of turbulence and a fully 3D description. A more complex model would also require more detailed experimental measurements; presently these are limited to the front position and could be extended to the thickness of the current (which can be obtained with limited accuracy with our present experimental setup) and to the velocity profiles (these are present only in a few literature experiments). More data can be obtained with numerical simulation, which however suffers the limitation that only low Reynolds number currents can be modeled.

This manuscript is structured as follows. The theoretical model is presented in Sec. II. The experimental layout and procedures and the actual experiments are described in Sec. III. Section IV contains the analysis of the experiments and a general discussion, while Sec. V includes some concluding remarks.

II. THEORETICAL MODEL

Consider a turbidity/particle-driven gravity current created by the release of a well-mixed monodispersed suspension into an ambient fluid of density ρ_a and propagating in the x-direction within a horizontal channel of uniform circular cross section, see Fig. 1. Gravity acts in the $-z$-direction.

The fluid of the current is considered to be a monodispersed suspension of density ρ_c generated by small heavy

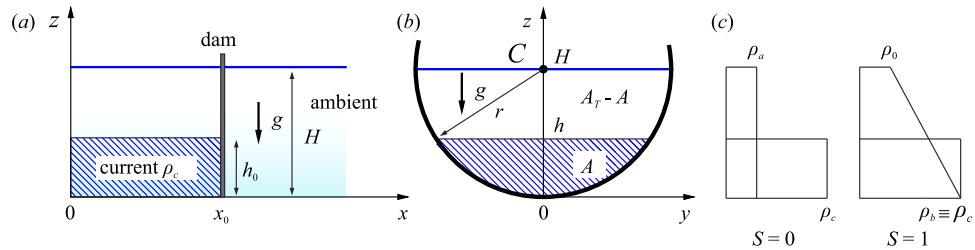

FIG. 1. A description of the (a) lock–release problem for the (b) circular cross section; (c) is the density profile for the case of homogeneous ambient fluid and linearly stratified ambient fluid, respectively. H is the ambient fluid depth, h_0 is the dense current height in the lock, x_0 is the lock length, A is the cross section area of the current, A_T is the total cross section area occupied by the fluid, $A_T - A$ is the cross section area occupied only by the ambient fluid, ρ_a is the mass density of the homogeneous ambient fluid, and ρ_0, ρ_b, and ρ_c are the mass density of the ambient fluid at $z = H$ and $z = 0$, respectively, and the mass density of the current.

particles of density ρ_p and diameter d_p, with an interstitial fluid of density ρ_i and kinematic viscosity ν. The concentration of the particles is expressed by the volume fraction $\kappa(x, z, t)$. The density of the current is

$$\rho_c = \rho_i(1 + \kappa\epsilon_p), \tag{1}$$

where

$$\epsilon_p = \frac{\rho_p - \rho_i}{\rho_i}. \tag{2}$$

The initial value of volume fraction κ_0 can be expressed as

$$\kappa_0 = \frac{\rho_{c0} - \rho_i}{\rho_p - \rho_i}, \tag{3}$$

where ρ_{c0} is the initial value of the mass density of the current (in the lock). In addition, we define the scaled volume fraction variable

$$\phi = \frac{\kappa}{\kappa_0}, \tag{4}$$

which is in the range [0, 1].

We first introduce the parameters and dimensionless numbers of our system. The x-lengths are scaled by the lock length x_0; the vertical z-lengths and the lateral y-lengths are scaled by the initial height of suspension in the lock h_0. The height of the ambient fluid is H. The geometry of the bottom cross section is a circle of radius r given by $f(z) = 2\sqrt{2rz - z^2}$, with a cross section area $A(z) = \int_0^z 2\sqrt{2rz' - z'^2}\,\mathrm{d}z'$ and the total cross section occupied by the fluid $A_T = \int_0^H f(z)dz$.

The scaled Stokes settling velocity of the particles β is defined by

$$\beta = \frac{W_s}{U}\frac{x_0}{h_0}, \tag{5}$$

where

$$W_s = \frac{1}{18}\epsilon_p g(1 - \kappa_0)^5 \frac{d_{p50}^2}{\nu}. \tag{6}$$

W_s is the settling speed of a small heavy particle of density ρ_p and median diameter d_{p50} (the midpoint of the grain-size distribution), and U is the reference velocity which is defined below. The parameter β compares the propagation time of the current for a distance x_0 to the particle settling time for a height h_0. The Reynolds number of the horizontal flow, $Re = h_N u_N/\nu$, where the subscript N denotes the value associated with the nose of the current, is assumed to be large.

We are interested in cases with small β, otherwise the particles settle out from the fluid during a relatively short propagation.

The flow is modeled by the one-layer shallow-water (SW) Boussinesq equations. The inviscid equations of motion, valid in both suspension and pure fluid regions, are the continuity equation, the momentum balance in the x-direction, and the conservation or "diffusion" equation for the volume fraction in the suspension.

Turbulent remixing is assumed: all the fluid of the initial current remains as part of the current in the domain $0 \le z \le h(x, t)$. The dispersed particles settle out from the current only at the bottom, with constant velocity calculated from the Stokes formula. The remaining non-settled particles are remixed vertically in the current so that the volume fraction is homogeneous over the cross section. At the interface $z = h(x, t)$, there is no relative motion between the current and the particles. The assumption of turbulent remixing, with a uniform concentration of the sediments in the cross section, is an approximation generally adopted[4] in order to reduce the complexity of the problem. Turbulence is assumed to be sufficient for remixing inside the current but not enough to favor entrainment and mixing with the ambient fluid. All these simplifications do not affect the correctness of the results in many practical situations; this is true even for more simplified models (see the work of Dade and Huppert[5] where a box model favourably compares with the experiments).

The shallow-water approximation provides the governing equations for the position of the interface h measured from the bottom line of the tank, the area-averaged velocity u of the dense fluid, and the area-averaged volume fraction variable ϕ as functions of t, and x for the cross section of circular form.

Two configurations are of interest: (i) the homogeneous, with the ambient fluid of a constant density ρ_a, and (ii) the stratified ambient. The formulation presented below for the homogeneous ambient fluid is based on the work of Zemach,[44] while the model for the stratified ambient fluid developed here is new. The modeling methodology has been detailed in previous papers; see the work of Ungarish[40] for a comprehensive review.

A. Homogeneous ambient fluid

We assume the density of the ambient fluid, ρ_a, constant and uniform. The scales for speed U and time T are

$$U = (\epsilon_p \kappa_0 g h_0)^{1/2}, \quad T = x_0/U, \quad \text{where} \quad \epsilon_p \kappa_0 \equiv \frac{\rho_{c0} - \rho_i}{\rho_i}. \tag{7}$$

We also use parameter δ,

$$\delta = \epsilon_i/(\epsilon_p \kappa_0), \quad \text{where} \quad \epsilon_i = (\rho_i - \rho_a)/\rho_a, \tag{8}$$

which represents the contribution of the interstitial fluid to the reduced gravity. We note that $\delta \to 0$ means that the intruding current is driven only by the particles and that the $\delta = 0$ case corresponds to the $\rho_i = \rho_a$ configuration, which was described by Zemach.[44]

The continuity, momentum, and conservation of the volume fraction in suspension equations in dimensionless form are

$$\begin{pmatrix} h_t \\ u_t \\ \phi_t \end{pmatrix} + \begin{pmatrix} u & \dfrac{A(h)}{f(h)} & 0 \\ \phi + \delta & u & h - \Psi(h) \\ 0 & 0 & u \end{pmatrix} \begin{pmatrix} h_x \\ u_x \\ \phi_x \end{pmatrix} = \begin{pmatrix} 0 \\ 0 \\ -\beta\phi \dfrac{f_M(h)}{A(h)} \end{pmatrix}, \tag{9}$$

where

$$\Psi(h) = \frac{\displaystyle\int_0^h z f(z)\,\mathrm{d}z}{\displaystyle\int_0^h f(z)\,\mathrm{d}z} \quad \text{and} \quad f_M(h) = \max[f(h), f(0)]. \tag{10}$$

Details on the derivation of $f_M(h)$ are included in the Appendix.

The system of partial differential equations (PDE) (9) is hyperbolic with characteristic relationships and trajectories given by

$$\begin{aligned} &\mathrm{d}h \pm \sqrt{\frac{A(h)}{f(h)(\phi+\delta)}}\,\mathrm{d}u + \frac{h - \Psi(h)}{(\phi+\delta)}\,\mathrm{d}\phi \\ &\quad = -\beta[h - \Psi(h)]\frac{f_M(h)}{A(h)}\frac{\phi}{\phi+\delta}\,\mathrm{d}t \\ &\mathrm{d}\phi = -\beta\phi\frac{f_M(h)}{A(h)}\,\mathrm{d}t \end{aligned} \quad \begin{aligned} &\text{on} \quad \frac{\mathrm{d}x}{\mathrm{d}t} = \lambda_\pm = u \pm \sqrt{(\phi+\delta)\frac{A(h)}{f(h)}}, \\ &\text{on} \quad \frac{\mathrm{d}x}{\mathrm{d}t} = \lambda_1 = u. \end{aligned} \tag{11}$$

The initial and boundary conditions are $h = 1$, $u = 0$, and $\phi = 1$ in the lock at $t = 0$, and $u = 0\ \forall t$ at the back wall $x = 0$. At the nose $x = x_N(t)$, we apply the extension of Benjamin's result[2] to the present flow field,[44]

$$u_N = (\phi + \delta)^{1/2} \chi Fr(a) h_N^{1/2}, \tag{12}$$

where $a = h_N/H$, $\chi \le 1$ is a coefficient taking into account the dissipation (this coefficient was not noticed by Zemach[44]), and $Fr(a)$ is the Froude number function defined for homogeneous gravity currents,[37]

$$Fr^2 = \frac{2(1-\varphi)}{1+\varphi}\left[1 - \varphi + \frac{1}{hA_T}\int_0^h z f(z)\,\mathrm{d}z\right], \quad \varphi = \frac{A}{A_T}. \tag{13}$$

The front condition (12) has been validated in the work of Zemach[44] with experimental data from Monaghan *et al.*[27] for $\delta = 0$.

B. Stratified ambient fluid

We assume that the density of the ambient fluid decreases linearly with z from ρ_b at the bottom of the tank to ρ_0 at its top (or open) surface. It is convenient to define an additional density ratio parameter using ρ_i as the reference density,

$$\epsilon_a = \frac{\rho_i - \rho_0}{\rho_0} \tag{14}$$

and

$$S = \frac{\rho_b - \rho_0}{\rho_i - \rho_0}. \tag{15}$$

The parameter S is in the range [0, 1] and represents the magnitude of stratification in the ambient fluid.

Next, we introduce a parameter Π,

$$\Pi = \kappa_0 \frac{\rho_p - \rho_i}{\rho_i - \rho_0}, \tag{16}$$

which compares the effect of particles' presence in the current to the stratification of the ambient fluid and is assumed to be positive. The model is restricted to the cases with $\rho_i \ge \rho_b > \rho_0$.

The reference speed U and time T are

$$U = (\epsilon_a g h_0)^{1/2}, \quad T = x_0/U. \tag{17}$$

The continuity, momentum, and conservation of the volume fraction in suspension equations in dimensionless form are

$$\begin{pmatrix} h_t \\ u_t \\ \phi_t \end{pmatrix} + \begin{pmatrix} u & \dfrac{A(h)}{f(h)} & 0 \\ \Pi\phi + 1 - S + S\dfrac{h}{H} & u & \Pi[h - \Psi(h)] \\ 0 & 0 & u \end{pmatrix} \begin{pmatrix} h_x \\ u_x \\ \phi_x \end{pmatrix} = \begin{pmatrix} 0 \\ 0 \\ -\beta\phi\dfrac{f_M(h)}{A(h)} \end{pmatrix}, \tag{18}$$

where $\Psi(h)$ and $f_M(h)$ are given by (10).

System (18) is hyperbolic and the eigenvalues of the matrix of coefficients are given by

$$\lambda_\pm = u \pm \sqrt{\frac{A(h)}{f(h)}\left(\Pi\phi + 1 - S + S\frac{h}{H}\right)}, \lambda_1 = u. \tag{19}$$

Consequently, the relationships between the variables on the characteristics are as follows:

$$\begin{cases} \mathrm{d}h \pm \sqrt{\dfrac{A(h)}{f(h)\left(\Pi\phi + 1 - S + S\dfrac{h}{H}\right)}}\mathrm{d}u \\ \qquad + \dfrac{\Pi[h-\Psi(h)]}{\Pi\phi + 1 - S + S\dfrac{h}{H}}\mathrm{d}\phi = -\beta\phi\dfrac{f_M(h)}{A(h)}\dfrac{\Pi[h-\Psi(h)]}{\Pi\phi + 1 - S + S\dfrac{h}{H}}\mathrm{d}t \quad \text{on} \quad \dfrac{\mathrm{d}x}{\mathrm{d}t} = \lambda_\pm, \\ \mathrm{d}\phi = -\beta\phi\dfrac{f_M(h)}{A(h)}\mathrm{d}t \quad \text{on} \quad \dfrac{\mathrm{d}x}{\mathrm{d}t} = \lambda_1. \end{cases} \tag{20}$$

The initial and boundary conditions are identical to those introduced for the homogeneous ambient fluid case: $h = 1$, $u = 0$, and $\phi = 1$ in the lock at $t = 0$, and $u = 0\ \forall t$ at the back wall $x = 0$. At the nose $x = x_N(t)$, we apply

$$u_N = \eta^{1/2}\chi Fr(a)h_N^{1/2}, \tag{21}$$

where

$$\eta = 1 + \Pi\phi - S\left[1 - \frac{1}{2}\frac{h_N}{H}(1+\gamma)\right], \tag{22}$$

$$\gamma = \frac{\displaystyle\int_0^{h_N}\frac{z}{h_N}(h_N - z)f(z)\,\mathrm{d}z}{\displaystyle\int_0^{h_N}(h_N - z)f(z)\,\mathrm{d}z}, \tag{23}$$

and $\chi \leq 1$ is a coefficient taking into account the dissipation.

For a stratified fluid, we define a buoyancy frequency $N^2 = -(g/\rho)\partial\rho/\partial z = Sg'/H$ and the celerity of the internal waves $c_w = Nr/(2\sqrt{2})$ (see Ref. 17).

To the best of our knowledge, the model developed here for the stratified ambient fluid is new and was not presented before. For $S \to 0$, the ambient fluid becomes homogeneous and the model becomes identical to the one from Sec. II A in the limits of the Boussinesq approximation. For $\Pi = 0$, the current becomes homogeneous (and so $k_0 = 0$) and the model reproduces the stratified model of Ungarish.[38]

C. Method of solution

We employ a two-step Lax-Wendroff finite-difference method (see Refs. 28 and 36 for details) to obtain $h(x,t)$, $u(x,t)$, $\phi(x,\ t)$, and $x_N(t)$. The variable length domain $[0,\ x_N]$ is transformed into a fixed domain [0, 1] by mapping the x-coordinate into $\eta = x/x_N(t)$. This method was successfully used for the particle-driven gravity currents in rectangular[4] and non-rectangular channels.[44]

The SW results displayed here were obtained with, typically, 200 grid points in the $[0, x_N]$ interval and a time step of 1×10^{-3} (convergence was also tested on finer grids).

As a check on the numerical results, a second code was developed based on the method of the characteristics. The equations have been integrated along the three trajectories with space step $\Delta x = 1/100$ or $\Delta x = 1/200$ and time step chosen in order to guarantee a Courant number $U\Delta t/\Delta x < 0.5$ (U is the flux velocity and usually $\Delta t = 1/100$). There is excellent agreement between the results of the two codes, which strengthens the confidence in the numerical values presented in this paper.

III. THE EXPERIMENTAL LAYOUT AND PROCEDURES

A series of lock–release experiments were performed at the Hydraulics Laboratory of the University of Parma to validate the model and gain more understanding and insight on the behaviour of particulate currents in non-rectangular and stratified configurations. To this end, a horizontal circular channel manufactured with polymethyl methacrylate (PMMA, a transparent thermoplastic) was employed to conduct tests with either the homogeneous or stratified ambient fluid. The channel has a length of 400 cm and an internal radius of 9.5 cm and includes at the upstream end a 27.5 cm long lock, separated from the downstream channel with a guillotine gate, see Fig. 2. In the partial-depth release tests, a horizontal lid moving in lateral guides was used to keep the intruding current properly separated from the upper layers before opening the lock. The separation was necessary because a vigorous mixing of the intruding current was necessary in order to guarantee an initial homogeneous suspension. Full mixing was obtained by moving a paddle (designed to induce small vortices) through a sheathed cable along the lock in the domain occupied by the mixture. Just before the opening of the gate, the lid was gently removed to limit the disturbances and a possible mixing at the interface between the sediment-laden fluid below and the upper ambient fluid. In the experiments with homogeneous ambient fluid, tap water treated with a softener and with density equal to $\rho = 0.998$ g cm^{-3} was used. In the experiments with stratified ambient fluid, saline was used, with a density profile varying linearly with depth from a minimum value close to $\rho = 1.000$ g cm^{-3} near the free surface to a maximum value near the bottom depending on the desired value of S. The stratification was obtained with an active control system:[17] a vane pump transferred saline from the first tank into the second "mixing" tank, initially containing softened tap water. Another vane pump transferred the mixture from the "mixing" tank to the bottom of the experimental tank through three pipes of 8 mm internal diameter. The use of small pipes accomplished a limited fluid velocity at the exit section, avoiding mixing, and a more uniform filling of the experimental channel. Both pumps were controlled in feedback by two electronic inverters; their flow rates, Q_1 and Q_2, were measured by two turbine meters and compared (and eventually corrected in real time acting on the inverters) with the theoretical values determined as the

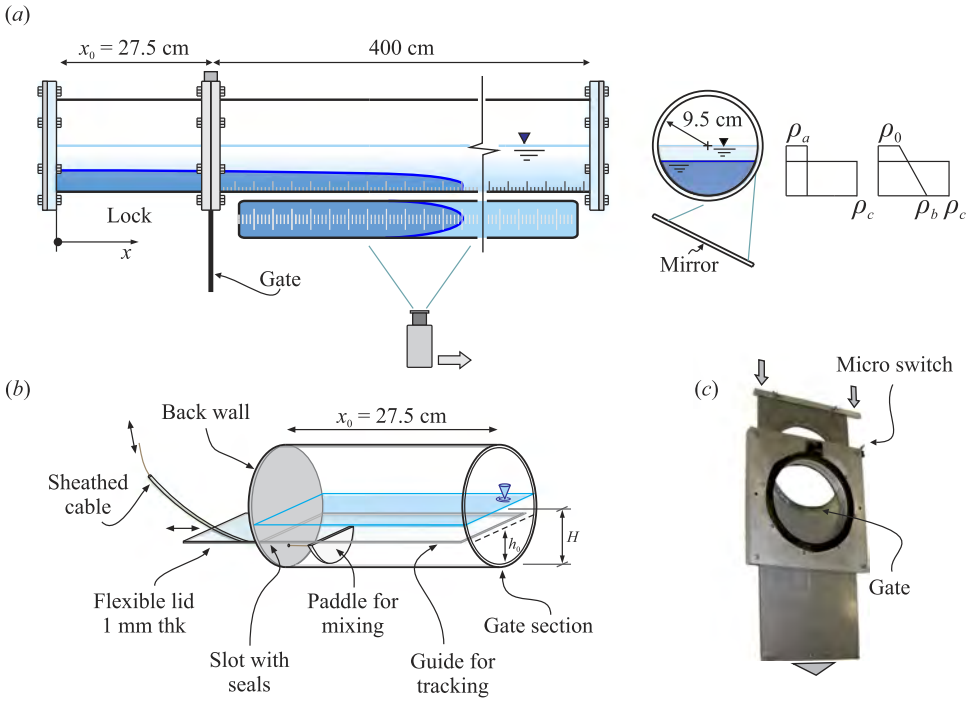

FIG. 2. Layout of the experimental setup. (a) The channel and the lock; (b) details of the lock with the movable horizontal lid and the paddle for remixing the particulate suspension before release; (c) the guillotine gate.

solution of an inverse problem based on mass continuity of the salt and of water.[12]

Upon completion of the channel filling, the density profile of the ambient fluid was measured and approximately 50 cm^3 of saline was extracted at 7 different depths using a syringe attached to a needle, whose tip was positioned with a vernier scale; the density of each sample was measured by a hydrometer, with an uncertainty of 10^{-3} g cm^{-3}. The agreement between the measures and the theoretical profile was generally good and within the expected uncertainties of the procedure. Figure 3 shows the normalized density profiles for some tests. The intruding fluid was obtained by adding particles of silicon carbide (SiC) of density ρ_p = 3.220 g cm^{-3} and d_{p50} = 8.1 μm and glass beads (GBs) of density ρ_p = 2.400 g cm^{-3} and d_{p50} = 24 μm, to an interstitial fluid (salt and water) of

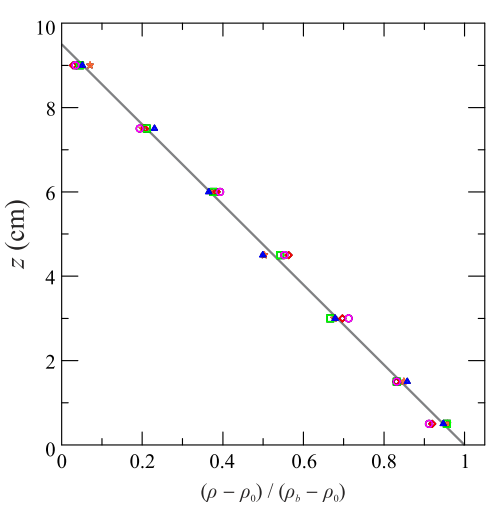

FIG. 3. Density profiles measured in the tank. The symbols refer to different experiments, and the straight line indicates perfect linearity.

density ρ_i = 0.998–1.065 g cm^{-3}. For some experiments with SiC particles, ρ_i was equal to the mass density of the ambient fluid, ρ_a; in all other tests, $\rho_i > \rho_a$ and, when a stratified ambient fluid was involved, $\rho_i \geq \rho_b$, where ρ_b is the mass density at the bottom of the ambient fluid. Some aniline dye was finally added to the whole mixture for an easy visualization of the front position of the current advancing in the transparent ambient fluid. Figure 4 shows the grain-size distributions of the particles measured with a particle sizer based on diffraction. Glass beads have a rounded shape, whereas silicon carbide particles have an angular shape (see Fig. 5). The shape of the particles has some effects on the settling, which has been considered to be of minor relevance with respect to the overall uncertainty in computing the settling speed. As to the settling speed given by (6), an alternative estimation can be obtained by experiments. Two different techniques were used: (i) laser Doppler velocimetry (LDV) in the dilute regime and (ii) image analysis of the interface separating clear fluid and sediment clouds in a vertical glass cylinder. A comparison of the estimated and measured values is shown in Table I for different combinations of the interstitial fluid density. Laser Doppler velocimetry gives results slightly in excess with respect to the theoretical Stokesian speed for SiC particles and with a large defect (more than 30%) for glass beads. The reason for this behaviour is not completely clear: presumably too large particles (glass beads are much larger than the space between fringes in the volume of measurements of the LDV system) generate a signal which is invalid for the electronics of the LDV system and are thus discarded from the statistics, which in turn is biased towards the smaller particles' speed values. The interface speed is the most realistic estimation since it reproduces the conditions during the actual experiments in the channel. Unfortunately it was impossible to estimate the interface speed for glass beads due to the limited contrast of the mixture (glass

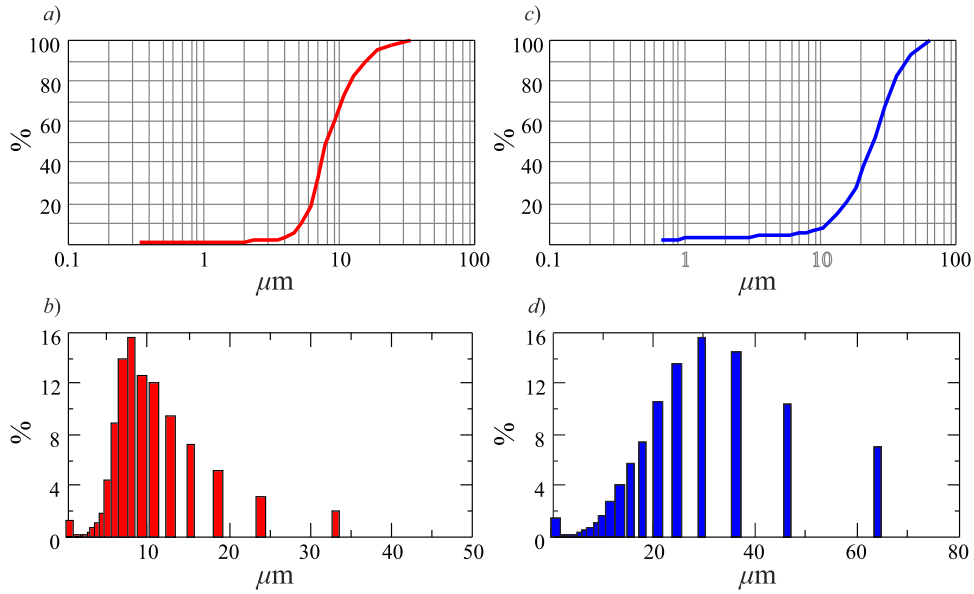

FIG. 4. Grain-size distribution of the particles. (a) Cumulative curve and (b) histogram for silicon carbide particles, $d_{p50} = 8.1\ \mu$m; (c) cumulative curve and (d) histogram for glass beads, $d_{p50} = 24\ \mu$m.

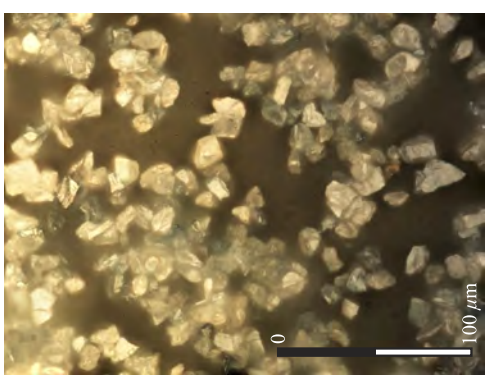

FIG. 5. A photograph of the SiC particles.

beads are almost transparent). Hence, we adopted the measured interface speed for SiC particles and the theoretical Stokesian speed for glass beads. The current fluid was gently poured inside the lock (27.5 cm long for all the tests). The experiments were carried out in full ($h_0 = H$) and partial-depth release, with the initial depth of the current being equal to 4.0-6.0 cm inside the lock, and a total depth of $H = r = 9.5$ cm, except for some experiments with homogeneous ambient fluid, which also exhibited a total depth of $H = 12$ cm. In the partial-depth experiments, the upper layer within the lock was soft water or linearly stratified fluid according to the characteristics of the ambient fluid in the downstream channel. The horizontal position of the channel was checked by an electronic level with 0.1° of accuracy.

In order to set the start of the flow, the opening of the gate could be detected by a micro-switch that switched on an LED when the gate was completely lifted. The gate took approximately 0.9 s to open completely and the time origin was signaled by the light of the LED.

Every experiment was recorded by a high-resolution video-camera (Canon Legria HF 20, 1920 × 1080 pixels) working at 25 frames per second (f.p.s.) and moving parallel to the tube so that the nose of the current was always in the field of view (FOV). High-frequency neon lights were used as a uniform and stable source of illumination. A 1 cm spaced grid was stuck at the bottom of the circular tube and reflected by mirrors providing a bottom view so as to detect the advancing front position of the current in time. With a specific software for a slow motion reproduction of the video (Adobe Premiere Pro CS6), it was possible to detect the interface between the current and the ambient fluid with 1/25 s accuracy, with data transcribed every 5 cm. Figure 6 shows the head of the current for test SH2, $Re_0 = 17.4 \times 10^3$ at $x/x_0 \approx 5$.

TABLE I. Settling speed of the particles in different configurations. ρ_p is the mass density of the particles, ρ_{c0} is the mass density of the mixture, κ_0 is the initial value of volume fraction of the particles, ρ_i and μ_i are the mass density and the dynamic viscosity of the interstitial fluid, respectively, W_s (th.) is the Stokesian theoretical speed, W_s (vc) is the estimate via the interface speed, and W_s (LDV) is the estimate via the laser Doppler velocimeter.

	ρ_p (g cm^{-3})	ρ_{c0} (g cm^{-3})	ρ_i (g cm^{-3})	μ_i (g cm^{-1} s^{-1}) (×10^{-2})	κ_0 (%)	W_s (th.) (cm s^{-1}) (×10^{-2})	W_s (vc) (cm s^{-1}) (×10^{-2})	W_s (LDV) (cm s^{-1}) (×10^{-2})
SiC in water	3.220	1.050	0.998	1.010	2.34	0.70	0.73	...
SiC in water		0.998	0.998	1.010	0.03	0.78	...	0.86
SiC in brine		1.080	1.065	1.227	0.70	0.61	0.64	...
GBs in water	2.400	0.998	0.998	1.010	0.07	3.57	...	2.21
GBs in brine		1.080	1.065	1.175	1.12	3.23	...	...

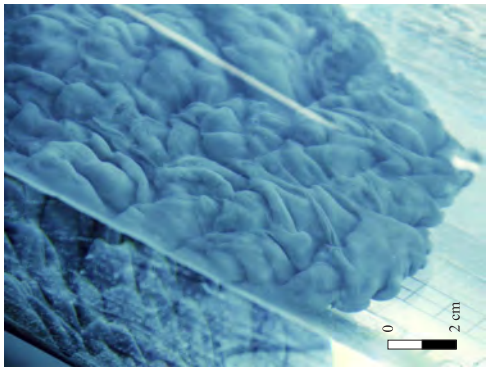

FIG. 6. The front of a gravity current of SiC particles in the homogeneous ambient fluid, Expt. SH2, $Re_0 = 17.4 \times 10^3$ at $x/x_0 \approx 5$. $Re_0 = Uh_0/\nu$, where U is the velocity scale, h_0 is the initial depth of the current in the lock, and ν is the kinematic viscosity.

A. Uncertainties

The mass density of the saline was measured with an accuracy of 10^{-3} g cm^{-3}, and the uncertainty for the parameter S is equal to $\Delta S/S = 2.1\%$–8%. The level of the ambient fluid was measured with an accuracy of 0.1 cm with an uncertainty $\Delta(h_0/H)/(h_0/H) \leq 4\%$. The velocity and time scales have uncertainty $\Delta U/U \leq 3.5\%$ and $\Delta T/T \leq 5\%$ for tests with a homogeneous ambient fluid and $\Delta U/U \leq 4.0\%$ and $\Delta T/T \leq 5.5\%$ for tests with a density stratified ambient fluid, respectively. With an uncertainty in the kinematic viscosity of the dense fluid equal to 2%, the Reynolds number has an uncertainty $\Delta Re_0/Re_0 \leq 8\%$. The uncertainty in the parameter β is $\Delta\beta/\beta \leq 8.5\%$. The uncertainty in the front speed $v_{N-\exp}$ is assumed to be equal to the uncertainty of the angular coefficient of the interpolating line and is $\leq 8\%$.

B. The experiments

Several experiments were carried out using two different types of particles and either the homogeneous or linearly density stratified ambient fluid. Tables II and III list the main parameters for the two sets of tests. For comparison, some saline experiments were also performed. The parameter β spans between 0.000 68 and 0.014 63 with an almost constant effective gravity, and the stratification parameter S varies from 0 (homogeneous ambient fluid) to 1. The Reynolds number ($Re_0 = Uh_0/\nu$) is in most instances large enough to insure pure turbulent flow even though for some tests its value was low enough ($Re_0 = 5100$) to suggest that the viscous effects are not completely negligible; this is a further approximation of the model adopted. The Reynolds number computed for experiments in the homogeneous ambient fluid with $\rho_i > \rho_a$ (GH1-GH6) spans between 2500 and 12 500, but it is not completely representative of the flux regime since the velocity scale U is computed with respect to $g' = g(\rho_{c0} - \rho_i)/\rho_i$, whereas referring U to $g' = g(\rho_{c0} - \rho_a)/\rho_a$ (a more representative value) yields a minimum value $Re_0 = 4800$, which corresponds to a well-developed turbulent regime. The tables also list the experimental front speed for the initial slumping phase, during which the current propagates with a constant height and velocity of the nose.

TABLE II. Parameters of the experiments with SiC particles (SH) and GBs (GH) in the homogeneous ambient fluid. "Hsal" stands for saline. d_{p50} is the median diameter of the particles, ρ_p is the density of the particles, ρ_{c0} is the initial density of the mixture, ρ_i is the density of the interstitial fluid, ρ_a is the density of the ambient fluid, $\epsilon_i = (\rho_i - \rho_a)/\rho_a$, $\epsilon_p = (\rho_p - \rho_i)/\rho_i$, $\delta = \epsilon_i/(\epsilon_p\kappa_0)$, $\kappa_0 = (\rho_{c0} - \rho_i)/(\rho_p - \rho_i)$, W_s is the settling speed of the particles, U is the velocity scale, g' is reduced gravity, $Re_0 = Uh_0/\nu$, T is the time scale, $v_{N-\exp}$ is the front speed of the current in the initial stage, and β is the scaled Stokes settling velocity of the particles.

Expt.	d_{p50} (μm)	ρ_p (g cm^{-3})	ρ_{c0} (g cm^{-3})	ρ_i (g cm^{-3})	ρ_a (g cm^{-3})	ϵ_i (%)	ϵ_p (%)	δ	κ_0 (%)	W_s (cm s^{-1}) ($\times 10^{-2}$)	H (cm)	h_0 (cm)	x_0 (cm)	U (cm s^{-1})	g' (cm s^{-2})	Re_0 ($\times 10^3$)	T (s)	$v_{N-\exp}$ (cm s^{-1})	$\beta(\times 10^{-3})$
SH1	8.1	3.220	1.050	0.998	0.998	0	222.65	0	2.34	0.73	12.0	12.0	27.5	24.8	51.1	24.8	1.111	11.0	0.68
SH2	8.1	3.220	1.050	0.998	0.998	0	222.65	0	2.34	0.73	9.5	9.5	27.5	22.0	51.1	17.4	1.248	10.9	0.96
SH3	8.1	3.220	1.050	0.998	0.998	0	222.65	0	2.34	0.73	9.5	6.0	27.5	17.5	51.1	8.8	1.571	9.3	1.91
SH4	8.1	3.220	1.050	0.998	0.998	0	222.65	0	2.34	0.73	12.0	6.0	27.5	17.5	51.1	8.8	1.571	10.5	1.91
SH5	8.1	3.220	1.050	0.998	0.998	0	222.65	0	2.34	0.73	9.5	4.0	27.5	14.3	51.1	4.8	1.924	9.1	3.51
SH6	8.1	3.220	1.050	0.998	0.998	0	222.65	0	2.34	0.73	12.0	4.0	27.5	14.3	51.1	4.8	1.924	8.8	3.51
Hsal	0	0	1.050	0.998	0.998	0	0	0	0	0	9.5	6.0	27.5	17.5	51.1	8.8	1.571	10.5	0
GH1	24	2.400	1.080	1.065	0.998	6.71	125.35	4.47	1.12	3.23	12.0	12.0	27.5	12.9	13.8	12.9	2.136	15.5	5.74
GH2	24	2.400	1.080	1.065	0.998	6.71	125.35	4.47	1.12	3.23	9.5	9.5	27.5	11.5	13.8	9.1	2.401	13.5	8.15
GH3	24	2.400	1.080	1.065	0.998	6.71	125.35	4.47	1.12	3.23	9.5	6.0	27.5	9.1	13.8	4.6	3.021	12.5	16.25
GH4	24	2.400	1.080	1.065	0.998	6.71	125.35	4.47	1.12	3.23	12.0	6.0	27.5	9.1	13.8	4.6	3.021	13.0	16.25
GH5	24	2.400	1.080	1.065	0.998	6.71	125.35	4.47	1.12	3.23	9.5	4.0	27.5	7.4	13.8	2.5	3.700	11.3	29.84
GH6	24	2.400	1.080	1.065	0.998	6.71	125.35	4.47	1.12	3.23	12.0	4.0	27.5	7.4	13.8	2.5	3.700	11.5	29.84

TABLE III. Parameters of the experiments with SiC particles (SS) and GBs (GS) in the stratified ambient fluid. "Ssal" stands for saline. ρ_0 and ρ_b are the density of the ambient fluid at $z = H$ and $z = 0$, respectively, $\epsilon_a = (\rho_i - \rho_0)/\rho_0$, $\Pi = \kappa_0(\rho_p - \rho_i)/(\rho_i - \rho_0)$, S is the stratification parameter, N is the buoyancy frequency, and c_w is the celerity of the internal waves. For the other symbols, see the caption of Table II.

Expt.	d_{p50} (μm)	ρ_p (g cm^{-3})	ρ_{c0} (g cm^{-3})	ρ_i (g cm^{-3})	ρ_0 (g cm^{-3})	ρ_b (g cm^{-3})	ϵ_a(%)	ϵ_p(%)	Π	κ_0(%)	S	N (s^{-1})	c_w (cm s^{-1})	W_s (cm s^{-1}) ($\times 10^{-2}$)	H (cm)	h_0 (cm)	x_0 (cm)	U (cm s^{-1})	g' (cm s^{-2})	Re_0 ($\times 10^3$)	T (s)	$v_{N-\exp}$ (cm s^{-1})	β ($\times 10^{-3}$)
SS1	8.1	3.220	1.068	1.049	1.005	1.049	4.38	206.96	0.432	0.88	1.00	2.13	7.1	0.64	9.5	9.5	27.5	20.2	42.9	16.0	1.362	9.5	0.92
SS2	8.1	3.220	1.069	1.050	1.005	1.050	4.48	206.67	0.422	0.88	1.00	2.15	7.2	0.64	9.5	6.0	27.5	16.2	43.9	8.1	1.694	8.3	1.80
SS3	8.1	3.220	1.080	1.065	1.007	1.053	5.76	202.35	0.259	0.70	0.79	2.17	7.3	0.64	9.5	9.5	27.5	23.2	56.5	18.3	1.187	10.7	0.80
SS4	8.1	3.220	1.080	1.065	1.007	1.052	5.76	202.35	0.259	0.70	0.78	2.15	7.2	0.64	9.5	6.0	27.5	18.4	56.5	9.2	1.494	9.7	1.59
SS5	8.1	3.220	1.080	1.065	1.005	1.053	5.97	202.35	0.250	0.70	0.80	2.22	7.5	0.64	9.5	4.0	27.5	15.3	58.5	5.1	1.797	8.0	2.88
SS6	8.1	3.220	1.080	1.065	1.005	1.042	5.97	202.35	0.250	0.70	0.62	1.95	6.5	0.64	9.5	9.5	27.5	23.6	58.5	18.7	1.166	11.4	0.79
SS7	8.1	3.220	1.080	1.065	1.006	1.041	5.86	202.35	0.254	0.70	0.59	1.90	6.4	0.64	9.5	6.0	27.5	18.6	57.5	9.3	1.480	10.4	1.58
SS8	8.1	3.220	1.080	1.065	1.004	1.041	6.08	202.35	0.246	0.70	0.61	1.95	6.6	0.64	9.5	4.0	27.5	15.4	59.6	5.1	1.781	9.2	2.85
SS9	8.1	3.220	1.080	1.065	1.005	1.029	5.97	202.35	0.250	0.70	0.40	1.57	5.3	0.64	9.5	9.5	27.5	23.6	58.5	18.7	1.166	11.9	0.79
SS10	8.1	3.220	1.080	1.065	1.005	1.032	5.97	202.35	0.250	0.70	0.45	1.67	5.6	0.64	9.5	6.0	27.5	18.7	58.5	9.4	1.467	10.8	1.57
SS11	8.1	3.220	1.080	1.065	1.006	1.027	5.86	202.35	0.254	0.70	0.36	1.47	4.9	0.64	9.5	4.0	27.5	15.2	57.5	5.1	1.813	10.0	2.90
Ssal1	0	0	1.080	1.065	1.006	1.053	7.36	0	∞	0	0.64	2.20	7.4	0	9.5	9.5	27.5	26.2	72.1	20.7	1.051	10.7	0
Ssal2	0	0	1.080	1.065	1.006	1.052	7.36	0	∞	0	0.62	2.17	7.3	0	9.5	6.0	27.5	20.8	72.1	10.4	1.322	10.0	0
GS1	24	2.400	1.080	1.065	1.006	1.050	5.86	125.35	0.254	1.12	0.75	2.12	7.1	3.23	9.5	9.5	27.5	23.4	57.5	18.5	1.177	10.1	4.00
GS2	24	2.400	1.080	1.065	1.006	1.052	5.86	125.35	0.254	1.12	0.78	2.17	7.3	3.23	9.5	6.0	27.5	18.6	57.5	9.3	1.480	9.2	7.96
GS3	24	2.400	1.080	1.065	1.006	1.053	5.86	125.35	0.254	1.12	0.80	2.20	7.4	3.23	9.5	4.0	27.5	15.2	57.5	5.1	1.813	8.0	14.63
GS4	24	2.400	1.080	1.065	1.006	1.041	5.86	125.35	0.254	1.12	0.59	1.90	6.4	3.23	9.5	9.5	27.5	23.4	57.5	18.5	1.177	10.9	4.00
GS5	24	2.400	1.080	1.065	1.007	1.042	5.76	125.35	0.259	1.12	0.60	1.89	6.4	3.23	9.5	6.0	27.5	18.4	56.5	9.2	1.494	10.0	8.03
GS6	24	2.400	1.080	1.065	1.006	1.041	5.86	125.35	0.254	1.12	0.59	1.90	6.4	3.23	9.5	4.0	27.5	15.2	57.5	5.1	1.813	8.3	14.63
GS7	24	2.400	1.080	1.065	1.006	1.032	5.86	125.35	0.254	1.12	0.44	1.63	5.5	3.23	9.5	9.5	27.5	23.4	57.5	18.5	1.177	11.3	4.00
GS8	24	2.400	1.080	1.065	1.004	1.026	6.08	125.35	0.246	1.12	0.36	1.50	5.1	3.23	9.5	6.0	27.5	18.9	59.6	9.5	1.454	11.2	7.82
GS9	24	2.400	1.080	1.065	1.004	1.029	6.08	125.35	0.246	1.12	0.41	1.60	5.4	3.23	9.5	4.0	27.5	15.4	59.6	5.1	1.781	10.0	14.37

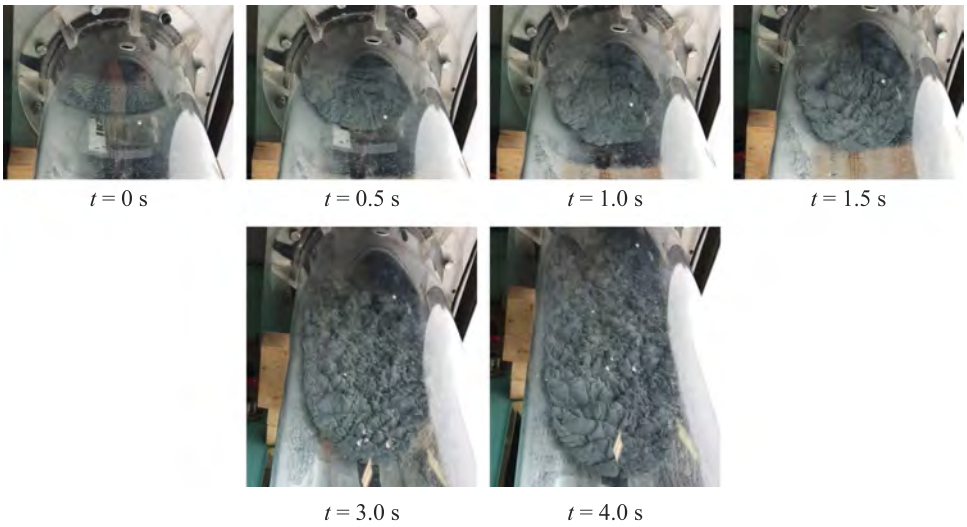

FIG. 7. Images of the current showing a progressive development of the interface geometry. Experiment SH2, SiC particles advancing in the homogeneous ambient fluid, top view.

Before comparing the model with the experiments, an overview of the geometric characteristics of the GCs can be helpful in clarifying the approximations of the model. Figure 7 shows six frames in the slumping phase, starting from the initial motion of the current, for a current advancing in a homogeneous ambient fluid. The front of the current looks characterized by numerous lobes interconnected and in rapid evolution. Their size decreases in the rear, where turbulence is growing with transfer of energy toward the smaller scales. The interface between the current and the ambient fluid is well defined. The flow is clearly three-dimensional, as can be better observed in the video in the supplementary material, which refers to this experiment.

Figure 8 shows four frames for the Experiment GH6. Each frame shows a side view and a bottom view of the current, with a time step of 3 s. The current becomes progressively thinner, the billows are less evident, and the wet perimeter (visible in the mirror) shrinks. The nose is well defined in all stages, with lobes shed also in the horizontal plane.

Figure 9 refers to a full-depth lock–release GC advancing in a stratified ambient fluid. The geometry of the body of the current is subject to a fast evolution, with the billows having an apparent vertical extent equal to the thickness of the current as observed on the curved surface of the circular cross section tank (the huge distortion does not allow a reliable direct estimation of the vertical extent of the current). A similar behaviour is also observed in Fig. 10, showing a glass bead GC advancing in a stratified ambient fluid.

IV. ANALYSIS OF THE RESULTS AND DISCUSSION

The comparison between the experimental position of the front of the current and the numerical model for tests with homogeneous ambient fluid is shown in Figs. 11 and 12 for SiC and GB particles, respectively, with a good reproduction of the initial slumping phase. However, after this stage, the error between the model and the data increases with time. A similar behaviour can be observed in Figs. 13 and 14 for SiC, and in Fig. 15 for GB particles in a linearly stratified ambient fluid.

The agreement is generally better for the full-depth than the partial-depth configuration. This is unexpected since the one-layer model adopted is based on hypotheses that are better satisfied for $h_0/H \rightarrow 0$. As a first possible explanation, we had initially conjectured that the mixing of the sediments before opening the lock, realized by shacking a

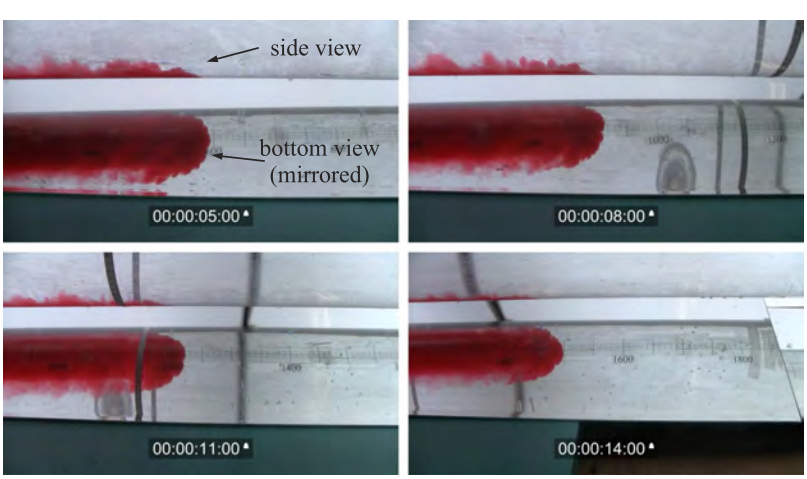

FIG. 8. A sequence of frames for the Experiment GH6, glass bead GC advancing in a homogeneous ambient fluid. Time step is 3 s.

FIG. 9. A sequence of frames for the Experiment SS9, full-depth lock–release SiC GC advancing in a stratified ambient fluid, $S = 0.40$. Time step is 5 s.

paddle parallel to the axis of the circular tank, was less effective in partial than full-depth configuration because the absence of the lid in the latter case allowed a direct access to the mixture in the lock, with the possibility of a more efficient mixing. This conjecture, however, is contradicted by two tests, presented in Figs. 14(f) and 14(g), featuring saline (which do not require remixing before opening the gate) advancing in a stratified ambient fluid and showing again better agreement between theory and experiments for the full-depth configuration.

A second possible explanation is connected to the Reynolds number, which progressively reduces for decreasing h_0/H. The effect of the Reynolds number can be explained as follows. For sediment-laden gravity currents at high Reynolds number, turbulence is sufficiently developed to guarantee a uniform sediment concentration in the vertical mixing, whereas a lower Reynolds number favours non-uniform mixing. The parameter controlling vertical mixing is the ratio between the settling speed of the particles and the root mean square vertical component of convective velocity (measured in the mid vertical level of the channel)[21] which, in turn, is related to the Reynolds number. The idea that the mechanism of sedimentation is one of the reasons of discrepancy between the model and experiments is corroborated by the different behaviour of experiments with SiC and GBs: in the SiC experiments (Fig. 11), the interstitial fluid has the same density of the ambient fluid and the reduced density depends only on sediment concentration ($\delta = 0$); in the GBs experiments (Fig. 15), sediments give a minor contribution to the reduced gravity since $\rho_i > \rho_a$ and $\delta = 4.7$. Since the error between the model and the experiments is less for GBs than for SiC experiments, we infer that the sediment concentration is a major cause of discrepancy.

In this respect, we notice that Monaghan *et al.*[26] also introduced a coefficient, already defined in the work of Martin and Nokes,[21] in the mass balance of sediments. It is also inferred that the height to length ratio of the lock affects the mixing of particulate currents from the head to the tail of the current, similar to saline gravity currents.[9] Essentially, the complex three-dimensional structure of the current is responsible for a vigorous mixing, which reduces the density, entrains the ambient fluid, and slows down the front. This three-dimensional structure is not captured by the present model, which, in turn, overestimates the speed of the current. The experiments by Hacker *et al.*[9] refer to full-depth lock–release with three different values of the ratio H/x_0, and the interpretation of the different experimental outcomes in the three cases also involved the reflected wave on the back wall and the possible disturbance effects induced by gate withdrawal. We can infer that the considerations developed in the work of Hacker *et al.*,[9] referred to the internal density structure of the current as modulated by the initial stage and to the progressive dilution effects, can be extended to the present experiments, where the ratio h_0/x_0 is a variable and the dynamics of the upper layer of the ambient fluid, present only in the partial-depth

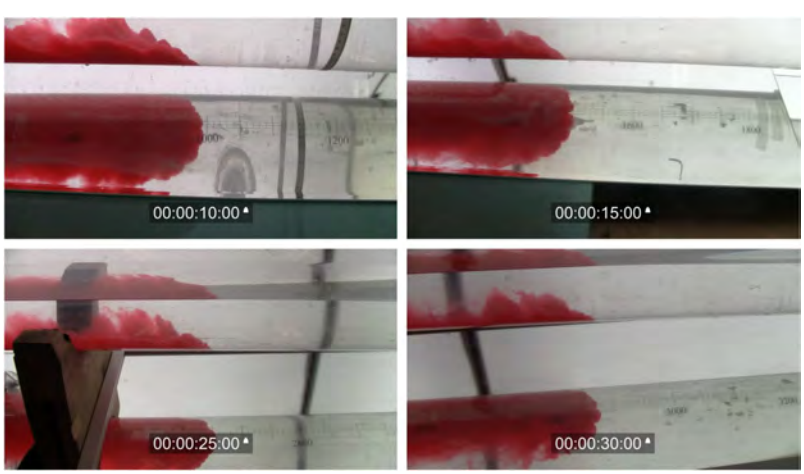

FIG. 10. A sequence of frames for the Experiment GS1, full-depth lock–release GB GC advancing in a stratified ambient fluid, $S = 0.75$. Time step is 5 s.

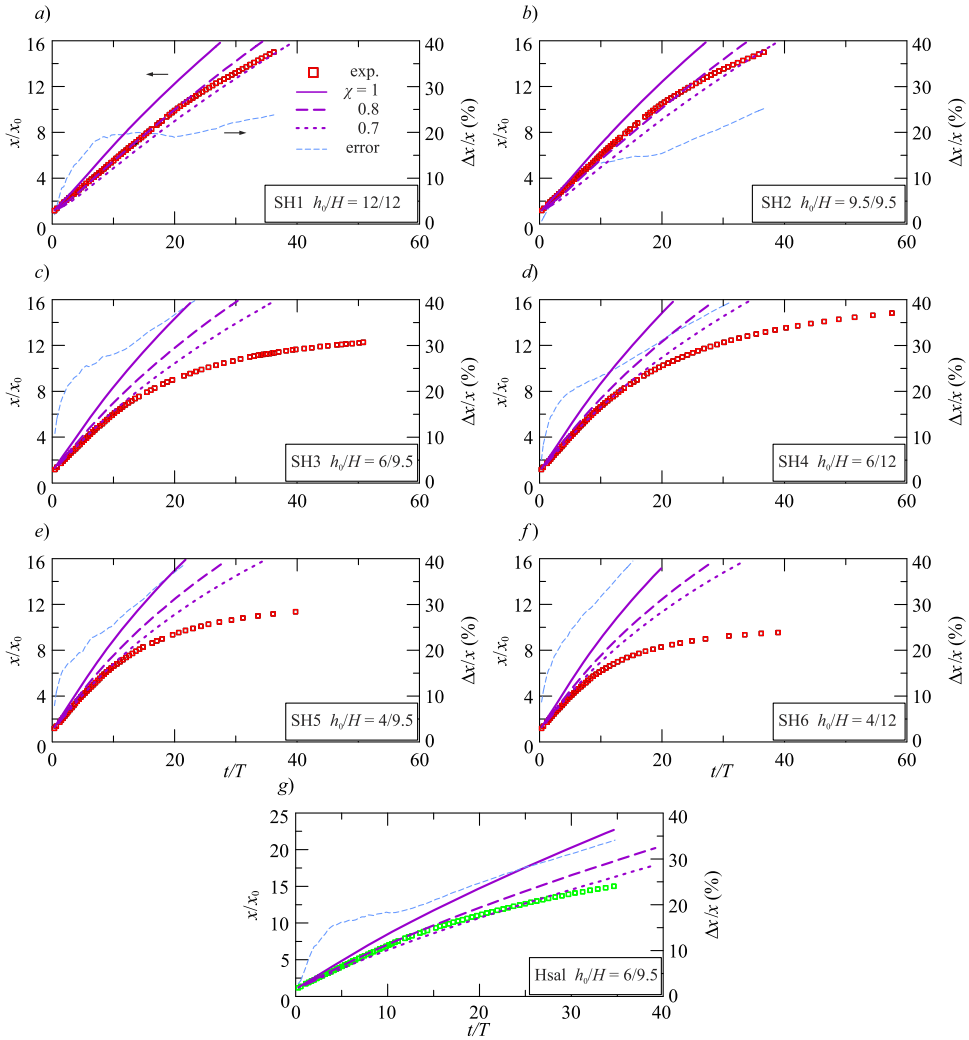

FIG. 11. Comparison between the experimental data and model prediction. [(a)–(f)] Particulate gravity currents with SiC in a homogeneous ambient fluid; (g) saline in a homogeneous ambient fluid. The symbols are the experimental data, and the line is the model with the coefficient multiplying the Froude number $\chi = 1$ (continuous), $\chi = 0.8$ (dashed), and $\chi = 0.7$ (dotted). The thin dashed line is the relative error, defined as $(x_{Nmodel} - x_{Nexp})/x_{Nexp}$, for the model prediction with coefficient $\chi = 1$ (values refer to the right vertical axis).

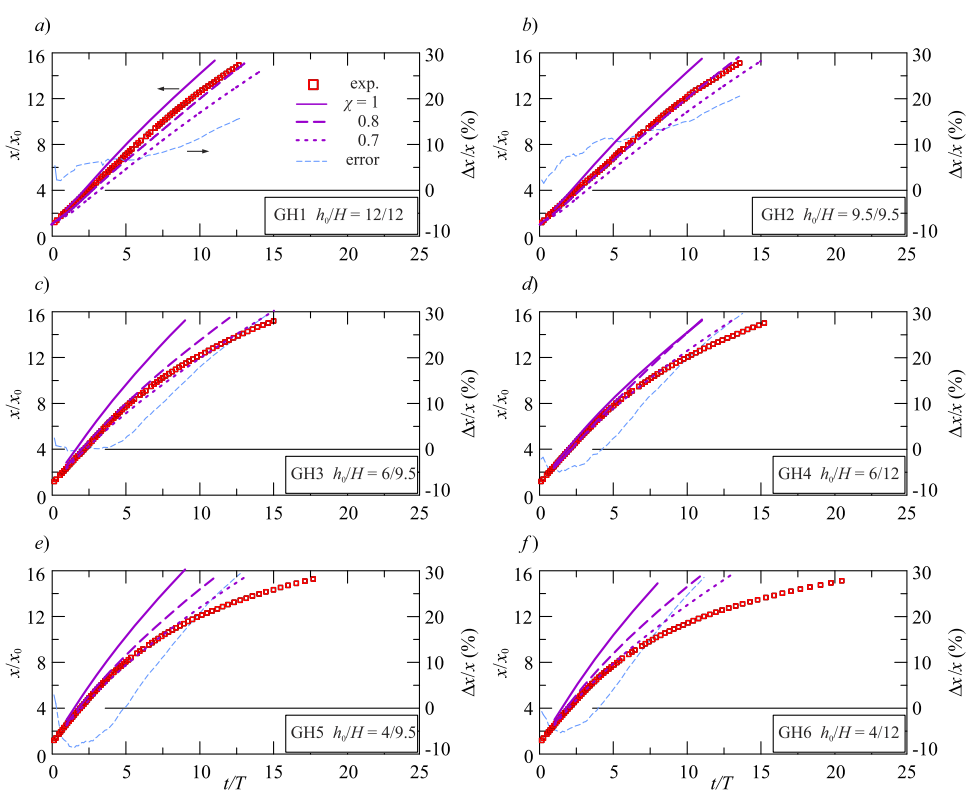

FIG. 12. Comparison between the experimental data and model prediction. [(a)–(f)] Particulate gravity currents with GBs in a homogeneous ambient fluid. For caption, see Fig. 11.

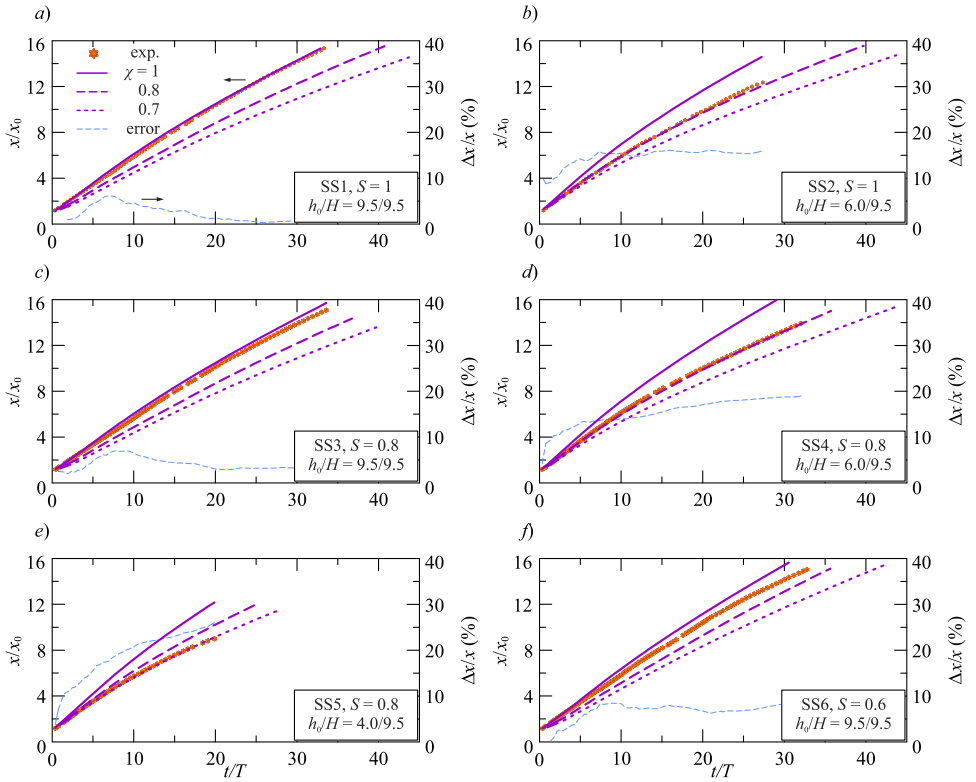

FIG. 13. Comparison between the experimental data and model prediction. [(a)–(f)] Particulate gravity currents with SiC particles in a linearly stratified ambient fluid. For caption, see Fig. 11.

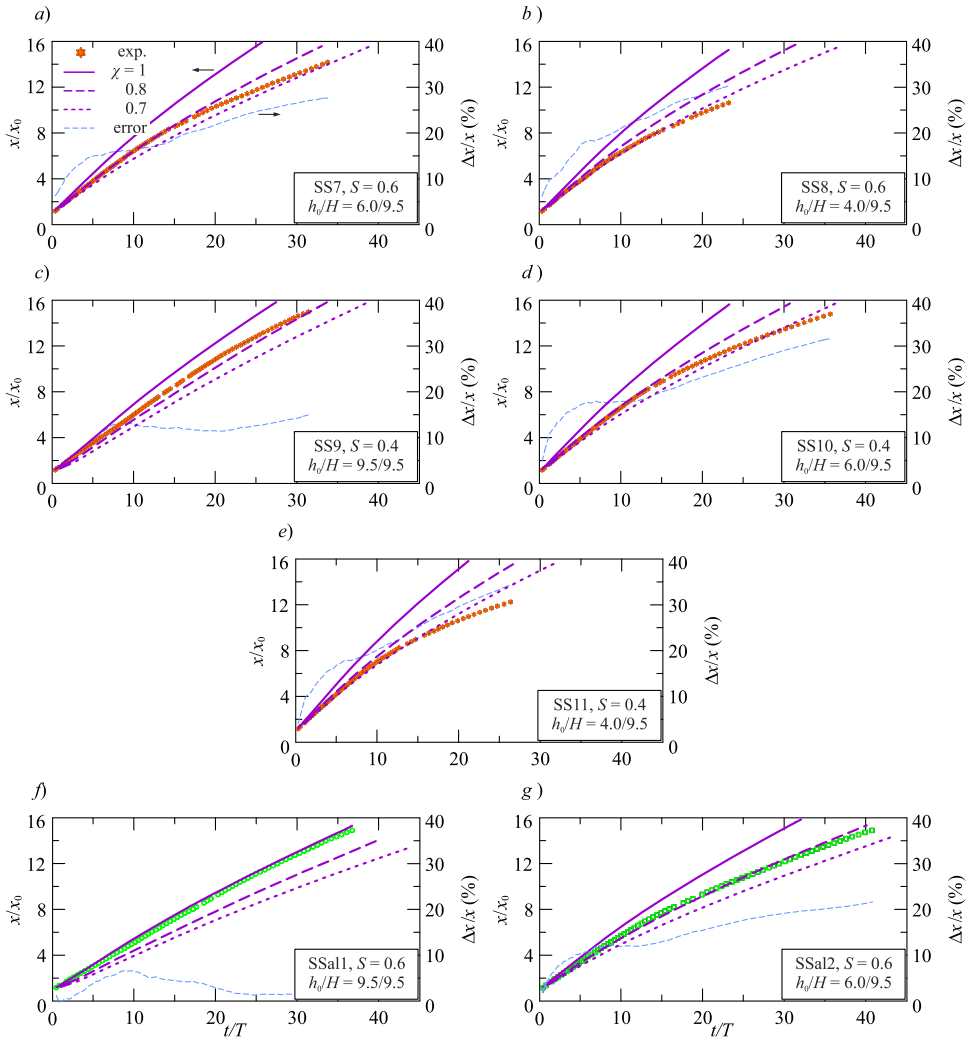

FIG. 14. Comparison between the experimental data and model prediction. [(a)–(e)] Particulate gravity currents with SiC particles in a linearly stratified ambient fluid; [(f)–(g)] saline in a linearly stratified ambient fluid. For caption, see Fig. 11.

case, contributes to render the current non-homogeneous in the vertical and horizontal directions of propagation.

We also notice that better agreement between the model and the experiments is obtained by using a Froude correction coefficient $\chi < 1$ (in most experiments with $\chi \in [0.7, 0.8]$) and that the initial phase is reproduced much better than the late stage of the current nose advancement. $\chi < 1$ is related to dissipation, which acts as a speed reducer equivalent to a density reduction of the current due to remixing.

Figures 13 and 14 show the comparison for SiC currents advancing in a linearly stratified ambient fluid. The interstitial fluid is always denser than that of the bottom density of the ambient fluid; hence, the reduced gravity is only partially due to the particles in suspension. As for the experiments with homogeneous ambient fluid, we found better agreement between experiments and theory for the full-depth [Figs. 13(a), 13(c), 13(f), and 14(c)] than for the partial-depth experiments [Figs. 13(b), 13(d), 13(e), 14(a), 14(b), 14(d), and 14(e)]. The agreement decreases for decreasing values of the stratification parameter S. To a lesser extent, this behaviour can also be observed for the experiments with GBs in a linearly stratified fluid, see Fig. 15, where the agreement reduces with the ratio h_0/H and with S. The coefficient χ which gives the best agreement between the model and experiments also decreases up to $\chi \approx 0.7$ for the experiment GS9, with the minimum value $h_0/H = 4.0/9.5$ and with $S = 0.4$. In all experiments, the model overpredicts the position of the advancing current, with a maximum relative error $(x_{Nmodel} - x_{Nexp})/x_{Nexp} \approx 30\%$, which is the usual value for most experiments with saline gravity currents. The interpretation of the discrepancy between theory and experiments is similar to that already provided for a homogeneous ambient, with the density stratification of the ambient fluid favouring the homogeneity of the intruding current, in particular for high values of the stratification parameter S.

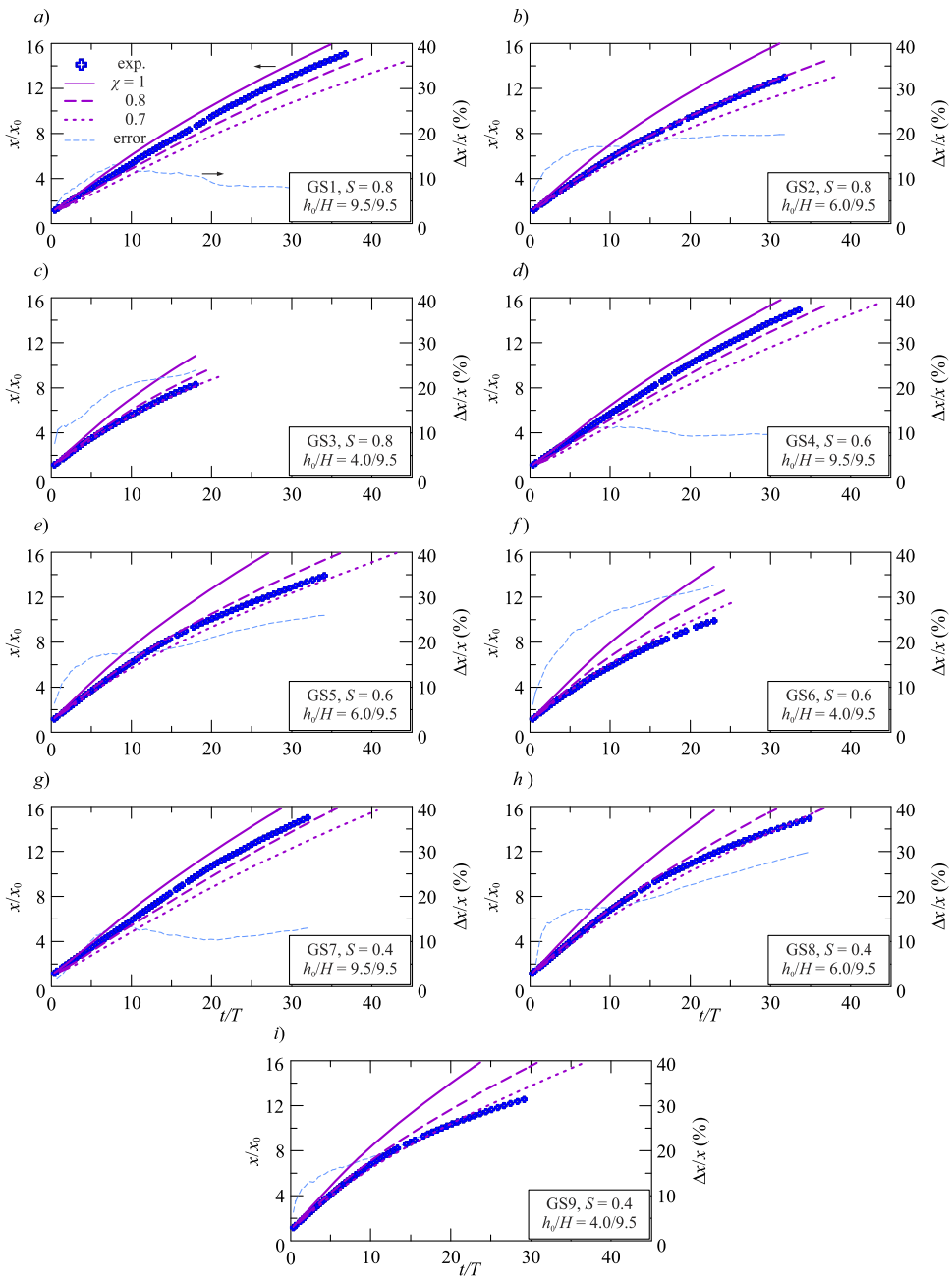

FIG. 15. Comparison between the experimental data and model prediction. [(a)–(i)] Particulate gravity currents with GBs in a linearly stratified ambient fluid. For caption, see Fig. 11.

A further source of uncertainty is due to the presence of internal waves. The currents are all supercritical in the initial stage ($v_{N-\exp} > c_w$, see Table III) and then turn to subcritical, with an interaction between current and internal waves. Coupling the front speed and the internal waves in order to understand the effects of the interaction requires a more sophisticated model than the simple one used here.

The simplicity of the model prevents the detailed description and interpretation of numerous aspects which are relevant in real full scale GCs. Interfacial turbulence, dissipation, mixing, entrainment, three-dimensional effects are all aspects which deserve attention in the future extension of the analysis. Numerical codes for fully 3D analysis (compulsory in non-rectangular cross section channels) are still far to be applied to GCs with adequate Reynolds number, and experiments seem quite promising in giving the proper hints for a better understanding of the processes. Nevertheless we believe that simple models, like those presented in this activity, can be helpful in capturing the analogies between "simple" and "complex" GCs and are expected to provide helpful insights.

V. CONCLUSIONS

We investigated the propagation of particulate gravity currents in lock–release configuration and advancing in a horizontal circular channel filled with a homogeneous or linearly stratified ambient fluid. A combined theoretical-experimental analysis was developed. The theoretical front position has been compared with experiments performed with particles having two different median diameters. When the ambient fluid is homogeneous, in some cases, the particles in suspension are fully causing the reduced gravity (i.e., the interparticle fluid has the same density as the ambient fluid and $\delta = 0$), while in other cases, the interparticle fluid is the main cause for the reduced gravity ($\delta > 0$ and particles in suspension are less important). The agreement with theory is fairly good for experiments with $\delta = 0$ in full-depth configuration ($h_0 = H$) and less good for experiments with $\delta > 0$. The discrepancy between theory and experiments is attributed to the description of the sedimentation process, which requires some adjustments in the settling data rate. We bear in mind the deliberate simplicity of the model, which with very limited computational efforts provides useful insights to the complex dynamics of these GCs, where entrainment, mixing, dissipation, turbulence, and stratification of the sediments give a complex scenario whose description is left for future analysis.

The better agreement obtained for full-depth than for partial-depth experiments is a consequence of remixing, which dilutes the intruding current with spatial variations in the vertical direction and along the direction of propagation. Experimental currents are always slower than their theoretical counterparts. The model developed is deliberately as simple as possible and does not include modeling of sedimentation or mixing. Dissipation is modeled simply by introducing a multiplicative coefficient $\chi < 1$ for the Froude number at the front of the current; this is sufficient to significantly improve the overlap between theory and experiments.

The currents advancing in a stratified ambient fluid show a similar behaviour: the agreement between the theoretical and the experimental front positions is good for full-depth experiments and less good for partial-depth experiments. In addition, the agreement decreases for decreasing values of the stratification parameter. We notice that in experiments with linearly stratified ambient fluid, the internal wave dynamics significantly influences all processes for both saline and particle laden gravity currents.

In general, the behaviour of a particle-driven (turbidity) gravity current is complicated by various effects that have no counterpart in the flow of a homogeneous (compositional-driven) current, such as unavoidable variations in shape and size of the dispersed material, re-suspension of already-settled particles, settling in the lock, and formation of clusters. As a consequence, the predictive power of simple models is reduced; the flows investigated in the present study are not an exception. Despite the discrepancies observed, we conclude that the extension/generalization of the shallow-water model to non-rectangular geometry, and specifically to a circular cross section, is useful. The quantitative discrepancies between the model prediction and the measurements are of the same order as for other previously tested geometries and are attributed to the underlying theoretical simplifications, irrespective of the cross section geometry. The models provide useful insights and estimates concerning the parametric influence and flow-field behaviour. Moreover, it was demonstrated that a simple adjustment of the nose-Froude condition with a coefficient in the range 0.7–0.8 renders fairly accurate predictions of the propagation speed. Therefore, the models constitute a useful tool in practical applications. This study also suggests future extensions for gravity current modeling, such as an extension of the present research to polydisperse gravity currents.

SUPPLEMENTARY MATERIAL

See supplementary material for a high-resolution video of the current in Experiment SH2, SiC particles in a homogeneous ambient fluid.

APPENDIX: AREA OF DEPOSITS FOR A CIRCULAR CROSS SECTION

To evaluate the volume-fraction balance equation for the dispersed particles, we have to compute the settling rate (see Ref. 27). Let us consider a generic cross section defined by the functions $y = f_1(z)$, $y > 0$, and $y = f_2(z)$, $y < 0$, and assume the direction of the settling velocity of the particles W_s to be vertical and identical across the section. For simplicity, let us initially consider a symmetric section with $f_1(z) = -f_2(z)$ and $f(z) = f_1(z) - f_2(z) \equiv 2f_1(z)$. The component of W_s locally orthogonal to the wall is $W_s \cos(\theta(z)) \equiv W_s f_1'/\sqrt{1+f_1'^2}$. The infinitesimal cross-sectional area from which mass deposit occurs in a time interval δt is $\mathrm{d}A_{dep} = 2W_s \cos(\theta)\,\mathrm{d}s\,\delta t$, where $\mathrm{d}s = \sqrt{1+f_1'^2}\,\mathrm{d}z$ is the infinitesimal length of the wall. Hence, $\mathrm{d}A_{dep} = 2W_s\,\mathrm{d}f_1\,\delta t$. The finite value A_{dep} is obtained by

$$A_{dep} = 2W_s\,\delta t \int_{f_1(a)}^{f_1(b)} \mathrm{d}f, \tag{A1}$$

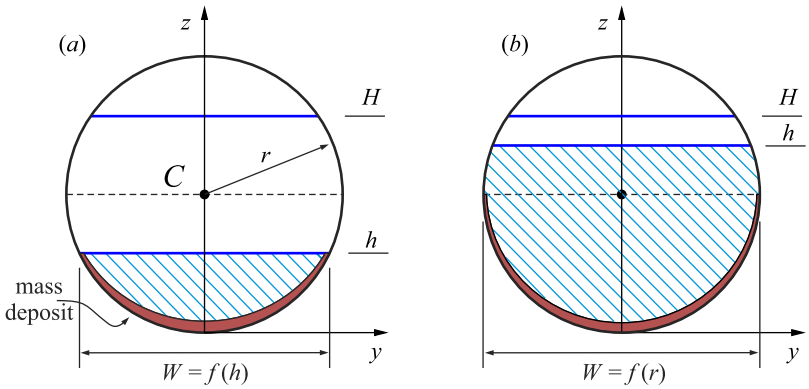

FIG. 16. Computation of the area of deposits for a circular cross section. (a) Case $h < r$ and (b) case $h > r$. The hatched area is the cross section of the current, and the brown area is the cross-sectional area of the sediment deposits.

where the extremes of integration must be chosen in order to only consider the portions of the wall which allow deposition of particles. The cross-sectional area of the current is $A(h)$ and the fraction of the mass of sediments deposited in the interval time δt is

$$\frac{\delta m}{m} = \frac{\text{Area of deposit}}{\text{Area of the current}} = -\frac{2W_s f_{1M}\delta t}{A(h)}. \tag{A2}$$

The term $2f_{1M}$ represents the length of the horizontal projection of the cross-sectional area of deposits. For a circular cross section, Fig. 16(a) shows the case $h < r$, where the width interested by deposition is $W = 2f_{1M} = f(h)$, and Fig. 16(a) shows the case $h > r$ with $W = 2f_{1M} = f(r)$. The results can be generalized by assuming $W = \max[f(z), z \in [0, h]]$.

The analysis can be extended with a similar approach to generic cross sections.

[1] Altinakar, M. S., Graf, W. H., and Hopfinger, E. J., "Flow structure in turbidity currents," J. Hydraul. Res. **34**(5), 713–718 (1996).
[2] Benjamin, T. B., "Gravity currents and related phenomena," J. Fluid Mech. **31**, 209–248 (1968).
[3] Bonnecaze, R. T., Hallworth, M. A., Huppert, H. E., and Lister, J. R., "Axisymmetric particle-driven gravity currents," J. Fluid Mech. **294**, 93–121 (1995).
[4] Bonnecaze, R. T., Huppert, H. E., and Lister, J. R., "Particle-driven gravity currents," J. Fluid Mech. **250**, 339–369 (1993).
[5] Dade, W. B. and Huppert, H. E., "A box model for non-entraining, suspension-driven gravity surges on horizontal surfaces," Sedimentology **42**(3), 453–470 (1995).
[6] Flinn, J. E. and Reimers, R. S., *Development of Predictions of Future Pollution Problems* (Supt. of Docs., US Govt. Print. Off., 1974), Vol. 3.
[7] Flynn, M. R., Ungarish, M., and Tan, A. W., "Gravity currents in a two-layer stratified ambient: The theory for the steady-state (front condition) and lock-released flows, and experimental confirmations," Phys. Fluids **24**(2), 026601 (2012).
[8] Garcia, M. H., "Depositional turbidity currents laden with poorly sorted sediment," J. Hydraul. Eng. **120**(11), 1240–1263 (1994).
[9] Hacker, J., Linden, P. F., and Dalziel, S. B., "Mixing in lock-release gravity currents," Dyn. Atmos. Oceans **24**(1–4), 183–195 (1996).
[10] Hay, A. E., "Turbidity currents and submarine channel formation in Rupert Inlet, British Columbia: 1. Surge observations," J. Geophys. Res.: Oceans **92**(C3), 2875–2881, doi:10.1029/jc092ic03p02875 (1987).
[11] Heezen, B. C. and Ewing, M., "Turbidity currents and submarine slumps, and the 1929 Grand Banks earthquake," Am. J. Sci. **250**(12), 849–873 (1952).
[12] Hill, F. D., "General density gradients in general domains: The 'two-tank' method revisited," Exp. Fluids **32**(4), 434–440 (2002).
[13] Hogg, A. J., Ungarish, M., and Huppert, H. E., "Particle-driven gravity currents: Asymptotic and box model solutions," Eur. J. Mech., B: Fluids **19**, 139–165 (2000).
[14] Huppert, H. E., "Quantitative modelling of granular suspension flows," Philos. Trans. R. Soc., A **356**, 2471–2496 (1998).
[15] Inman, D. L., Nordstrom, C. E., and Flick, R. E., "Currents in submarine canyons: An air-sea-land interaction," Annu. Rev. Fluid Mech. **8**(1), 275–310 (1976).
[16] Kneller, B. and Buckee, C., "The structure and fluid mechanics of turbidity currents: A review of some recent studies and their geological implications," Sedimentology **47**(s1), 62–94 (2000).
[17] Longo, S., Ungarish, M., Di Federico, V., Chiapponi, L., and Addona, F., "Gravity currents in a linearly stratified ambient fluid created by lock release and influx in semi-circular and rectangular channels," Phys. Fluids **28**(9), 096602 (2016).
[18] Longo, S., Ungarish, M., Di Federico, V., Chiapponi, L., and Addona, F., "Gravity currents produced by constant and time varying inflow in a circular cross-section channel: Experiments and theory," Adv. Water Resour. **90**, 10–23 (2016).
[19] Longo, S., Ungarish, M., Di Federico, V., Chiapponi, L., and Maranzoni, A., "The propagation of gravity currents in a circular cross-section channel: Experiments and theory," J. Fluid Mech. **764**, 513–537 (2015).
[20] Marino, B. M. and Thomas, L. P., "Dam-break release of a gravity current in a power-law channel section," J. Phys.: Conf. Ser. **296**, 012008 (2011).
[21] Martin, D. and Nokes, R., "A fluid-dynamical study of crystal settling in convecting magmas," J. Petrol. **30**(6), 1471–1500 (1989).
[22] Maxworthy, T., Leilich, J. S. J. E., Simpson, J. E., and Meiburg, E. H., "The propagation of a gravity current into a linearly stratified fluid," J. Fluid Mech. **453**, 371–394 (2002).
[23] Mériaux, C. A. and Kurz-Besson, C. B., "A study of gravity currents carrying polydisperse particles along a V-shaped valley," Eur. J. Mech., B: Fluids **63**, 52–65 (2017).
[24] Mériaux, C. A., Zemach, T., Kurz-Besson, C. B., and Ungarish, M., "The propagation of particulate gravity currents in a V-shaped triangular cross section channel: Lock-release experiments and shallow-water numerical simulations," Phys. Fluids **28**, 036601 (2016).
[25] Mohrig, D. and Buttles, J., "Deep turbidity currents in shallow channels," Geology **35**(2), 155–158 (2007).
[26] Monaghan, J. J., Mériaux, C. A., Huppert, H. E., and Mansour, J., "Particulate gravity currents along V-shaped valleys," J. Fluid Mech. **631**, 419–440 (2009).
[27] Monaghan, J. J., Mériaux, C. A., Huppert, H. E., and Monaghan, J. M., "High Reynolds number gravity currents along V-shaped valleys," Eur. J. Mech., B: Fluids **28**(5), 651–659 (2009).
[28] Morton, K. W. and Mayers, D. F., *Numerical Solution of Partial Differential Equations: An Introduction* (Cambridge University Press, 2005).
[29] Normark, W. R. and Dickson, F. H., "Man-made turbidity currents in lake superior," Sedimentology **23**(6), 815–831 (1976).
[30] Perrodon, A., *Dynamics of Oil and Gas Accumulations* (TECHNIP, 1983), Vol. 5.
[31] Seymour, R. J., "Neashore auto-suspending turbidity flows," Ocean Eng. **13**(5), 435–447 (1986).
[32] Simpson, J. E., "Gravity currents in the laboratory, atmosphere, and ocean," Annu. Rev. Fluid Mech. **14**, 213–234 (1982).
[33] Simpson, J. E., *Gravity Currents in the Environment and the Laboratory* (Cambridge University Press, 1997).

[34]Sparks, R. S. J., Bonnecaze, R. T., Huppert, H. E., Lister, J. R., Hallworth, M. A., Mader, H., and Phillips, J., "Sediment-laden gravity currents with reversed buoyancy," Earth Planet. Sci. Lett. **114**, 243–257 (1993).
[35]Ungarish, M., "On gravity currents in a linearly stratified ambient: A generalization of Benjamin's steady-state propagation results," J. Fluid Mech. **548**, 49–68 (2006).
[36]Ungarish, M., *An Introduction to Gravity Currents and Intrusions* (Chapman and Hall/CRC Press, Boca Raton, London, New York, 2009).
[37]Ungarish, M., "A general solution of Benjamin-type gravity current in a channel of non-rectangular cross-section," Environ. Fluid Mech. **12**(3), 251–263 (2012).
[38]Ungarish, M., "Gravity currents and intrusions of stratified fluids into a stratified ambient," Environ. Fluid Mech. **12**(2), 115–132 (2012).
[39]Ungarish, M., "Two-layer shallow-water dam-break solutions for gravity currents in non-rectangular cross-area channels," J. Fluid Mech. **732**, 537–570 (2013).
[40]Ungarish, M., "Thin-layer models for gravity currents in channels of general cross-section area, a review," Environ. Fluid Mech. (published online).
[41]Ungarish, M. and Huppert, H. E., "On gravity currents propagating at the base of a stratified ambient," J. Fluid Mech. **458**, 283–301 (2002).
[42]Ungarish, M., Mériaux, C. A., and Kurz-Besson, C. B., "The propagation of gravity currents in a V-shaped triangular cross-section channel: Experiments and theory," J. Fluid Mech. **754**, 232–249 (2014).
[43]Yih, C.-S., *Stratified Flows* (Elsevier, 2012).
[44]Zemach, T., "Particle-driven gravity currents in non-rectangular cross section channels," Phys. Fluids **27**, 103303-1–103303-21 (2015).